AIAA Journal, Available online 2 April 2023
DOI:10.2514/1.J062365

Flow and Noise Predictions of the Isolated Subsonic Jets from the Doak Laboratory Experiment

Vasily Gryazev,[1] Annabel P. Markesteijn,[2] Sergey A. Karabasov,[3]
Queen Mary University of London, London, England, E1 4NS, United Kingdom

Jack L. T. Lawrence,[4]
University of Southampton, Southampton, England, SO17 1BJ, United Kingdom

and
Anderson R. Proença [5]
Cranfield University, Cranfield, England, MK43 0AL, United Kingdom

Large Eddy Simulations (LES) are performed for two isolated unheated jet flows corresponding to a Doak Laboratory experiment performed at the University of Southampton. The jet speeds studied correspond to acoustic Mach numbers 0.6 and 0.8, and Reynolds number based on the nozzle exit diameter of about 1 million. The LES method is based on the Compact Accurately Boundary-Adjusting High-Resolution Technique (CABARET) and is implemented on Graphics Processing Units (GPU) to obtain 1000-1100 convective time units for statistical averaging with reasonable run times. In comparison with the previous jet LES calculations with the GPU CABARET method, meanflow velocity and turbulent intensity profiles are matched with the hot-wire measurements just downstream of the nozzle exit. The far-field noise spectra of the Doak jets are evaluated using two methods, the Ffowcs Williams–Hawkings approach and a reduced-order implementation of the Goldstein Generalised Acoustic Analogy. The flow and noise results are compared with hot-

[1] Post-Doctoral Researcher, School of Engineering and Material Sciences, Mile End Road, London, E1 4NS, UK. Member AIAA
[2] Post-Doctoral Researcher, School of Engineering and Material Sciences, Mile End Road, London, E1 4NS, UK; also, Research Scientist/Director, GPU-Prime Ltd., 16 St. Thomas Close, Comberton, Cambridge, England CB23 7DN, United Kingdom. Member AIAA.
[3] Professor, School of Engineering and Material Sciences, Mile End Road London, E1 4NS, UK; also, Research Scientist/Director, GPU-Prime Ltd., 16 St. Thomas Close, Comberton, Cambridge, England CB23 7DN, United Kingdom. Associate Fellow AIAA.
[4] Senior Research Fellow, Institute of Sound and Vibration Research, Highfield, Southampton SO17 1BJ, Member AIAA
[5] Lecturer in Aerodynamics, School of Aerospace, Transport and Manufacturing, Cranfield, MK43 0AL, Member AIAA.

wire and acoustic microphone measurements of the Doak Laboratory and critically analysed in comparison with the NASA SHJAR data base.

I. Introduction

DESPITE decades of research, jet noise remains an active area in aeroacoustics [1-5]. Due to advances in high-resolution algorithms and computer architectures, Large Eddy Simulations (LES) have become increasingly popular for high-resolution jet flow and noise calculations [6-9]. However, it has long been known that the difference in inflow conditions may play a role in the jet development [10, 11], thereby, resulting in differences between the jet flow and, possibly, the generated far-field noise between experimental datasets corresponding to different facilities and also between the LES and the experiment.

There are relatively few high-quality jet noise databases, where both the flow data and the far-field acoustic measurements are available. One of them, the so-called SHJAR (Small Hot Jet Acoustic Rig) [12,13] at NASA has attracted significant attention for validation of LES methods [14-17] as well as hybrid Reynolds Averaged Navier–Stokes (RANS)–LES approaches [18-21]. In addition to conventional fixed-grid Navier-Stokes methods, alternative unsteady Computational Fluid Dynamics (CFD) methods of particle-in-cell type such as Lattice Boltzmann (LBM) were tested and showed their computational efficiency for flow and noise predictions for the NASA jet noise problems [22, 23].

Despite the abundance of various LES jet noise studies in the literature, there is only a few well-documented datasets, which include not only the jet flow and far-field noise solutions, but also are the jet inflow condition comparisons with the same experiment. Furthermore, to the best knowledge of the authors, the only fully documented jet noise case, which includes the well-defined upstream conditions for the jet meanflow and turbulence is the experiment of the University of Poitiers, which was used in a series of LES-based analyses of the jet noise mechanisms by the Poitiers-CalTech group [24, 25].

The objective of the current work is to expand the publicly available database of fully documented jet noise experiment and LES cases. The current investigation is centred around results of the recent experimental test campaign, conducted in the Doak Laboratory at the University of Southampton [3-5]. The Doak jets are unheated and issue from a convergent profiled nozzle at an acoustic Mach number (the ratio of the jet velocity at the nozzle exit to

the far-field sound speed) of 0.6 and 0.8, The Reynolds numbers of the Doak jets based on the nozzle exit diameter and the jet exit velocity are 7×10^5 and 9×10^5, which are close to the NASA SHJAR jet cases.

For the Mach 0.6 Doak jet, an eddy-resolving simulation of flow and noise was already performed in [26] using a hybrid RANS-LES approach coupled with the Ffowcs Williams – Hawkings (FW-H) method with several penetrable control surfaces and closing disks [6, 27]. However, the first work on the Doak jet cases also left several questions unanswered. For example, it was unclear how well the jet inflow conditions of the experiment were matched in the LES calculation. Furthermore, some discrepancies between the far-field noise spectra predicted from the LES and the experiment were observed at low and high frequencies (Fig.11 in [26]). In particular, at the 40° observer angle measured relative to the downstream jet axis, which is close to the peak jet noise direction where the experimental data are available, a reasonable 2-3dB accuracy of noise spectra predictions was reported for the frequency range of $0.08 < St_D < 2$, where the jet Strouhal number, $St_D = fD_j / U_j$ is based on the jet nozzle diameter D_j and nozzle exit velocity U_j. However, at the same time, the jet noise spectra predictions at the 90° polar angle showed a 3-4 dB error for the intermediate frequency range of $0.08 < St_D < 0.4$ and a prominent (~5dB amplitude) discrete tone at $St_D \sim 0.8$, which was not observed in the experiment. It can be noted that acoustic tones are typical of transitional jet shear layers, however, they are not expected in high-speed jets at the Reynolds number of around one million. Hence, the goal of the current investigation is to perform a series of LES calculations, which are sufficiently well-resolved in the jet shear layers and statistically converged to capture low frequencies. The calculations will correspond to the inflow boundary condition, which accurately matches conditions of the Doak experiment. By refining the LES grid in this well-defined jet case, the goal is also to extend the high-frequency limit of accurate jet noise calculations to the jet Strouhal number of around 10. To assess the Mach number effects, both the Doak jets corresponding to acoustic Mach numbers 0.6 and 0.8 will be considered.

The simulations in the present work are based on the Compact Accurately Boundary-Adjusting high-REsolution Technique (CABARET) method developed by the authors in a series of previous works [28-30]. CABARET is a shock-capturing scheme with improved dissipation and dispersion properties as well as the asynchronous time stepping [31]. The governing compressible Navier-Stokes equations are solved in the Monotonically Integrated LES (MILES) framework [9], and the solution process was implemented on Graphics Processing Units (GPU) to speed up the turnaround time to 2-3 days on LES grids consisting of 100-120 million cells [17, 32-34]. An equilibrium wall

model and a synthetic turbulence inflow condition were used to mimic the effect of the nozzle wall and the flow development upstream of the nozzle exit. Details of both these models can be found in [34]. The OpenFOAM snappyHexMesh utility was used for generating patches of high-quality Cartesian grid isotopically refined in the location of early shear layers following our previous experience with the NASA SHJAR jets [17]. For the far-field noise calculations, the penetrable-surface formulation of the Ffowcs Williams-Hawkings (FW-H) method with multiple closing disks is applied using the well-tested numerical procedure to remove pseudo sound caused by multiple vorticity waves crossing the acoustic integration surface [6, 9, 18]. In comparison with the previous jet flow and noise simulations performed with the CABARET method, the distinct novelty here is that the inflow jet boundary conditions are tailored to accurately represent both the time-averaged velocity and the turbulence intensity profiles measured just downstream of the nozzle exit. By doing so, it will be examined if it is sufficient to match the two commonly considered statistical properties just downstream of the nozzle exit to describe both the jet flow development and the far-field noise of the Doak jets. In addition to comparing the LES predictions to the Doak experiment, the results will also be analysed in comparison with predictions of the sJet method [35], which is an empirical model obtained from interpolations over the NASA SHJAR dataset.

Another goal of the present study is to calculate the far-field noise of the same Doak jets by applying a reduced-order model based on acoustic analogy, where single-point time-averaged flow quantities and turbulence kinetic energy are extracted from the LES. In comparison with the FW-H method, the reduced-order model does not require unsteady information about the flow, which makes it compatible with the fast steady CFD methods such as those solving Reynolds Averaged Navier Stokes (RANS) equations [36, 37]. Specifically, following Goldstein [38-40], a reduced-order version of the Generalised Acoustic Analogy (GAA) was implemented for the Doak jets. A distinct feature of the GAA model is that it considers several components of the fluctuating turbulent Reynolds stresses. These components correspond to different acoustic directivities of the effective jet noise source. The amplitudes of the components of the Reynolds stress auto-covariance are here assumed to be the same as those of the single-stream jets in [36, 41, 42]. In addition, the reduced order model uses a set of non-dimensional proportionality parameters to represent acoustic length and time scales, which in [37] were also found relatively unsensitive to the jet case. The assumption of applicability of the previously obtained correlation amplitude, length scale, and time scale parameters will be re-examined for acoustic modelling of the Doak jets.

II. Experimental Setup and Comparison with the NASA SHJAR Dataset

The Institute of Sound and Vibration Research (ISVR) Doak Laboratory is an anechoic chamber, fully anechoic down to a frequency of 400 Hz. The facility has dimensions approximately of 15 m length by 7 m width by 5 m height. A core air jet is supplied by a high-pressure compressor–reservoir system. Single-stream jet measurements can be performed on flow regimes characteristic of civil aircraft and for 1⁄50th-scale experiments. The jet rig can achieve a controlled exit acoustic Mach number range of between 0.15 and 1. Further information regarding the Doak Flight Jet Rig (FJR) can be found in [3-5] and photographs of the Doak FJR facility are shown in Fig.1.

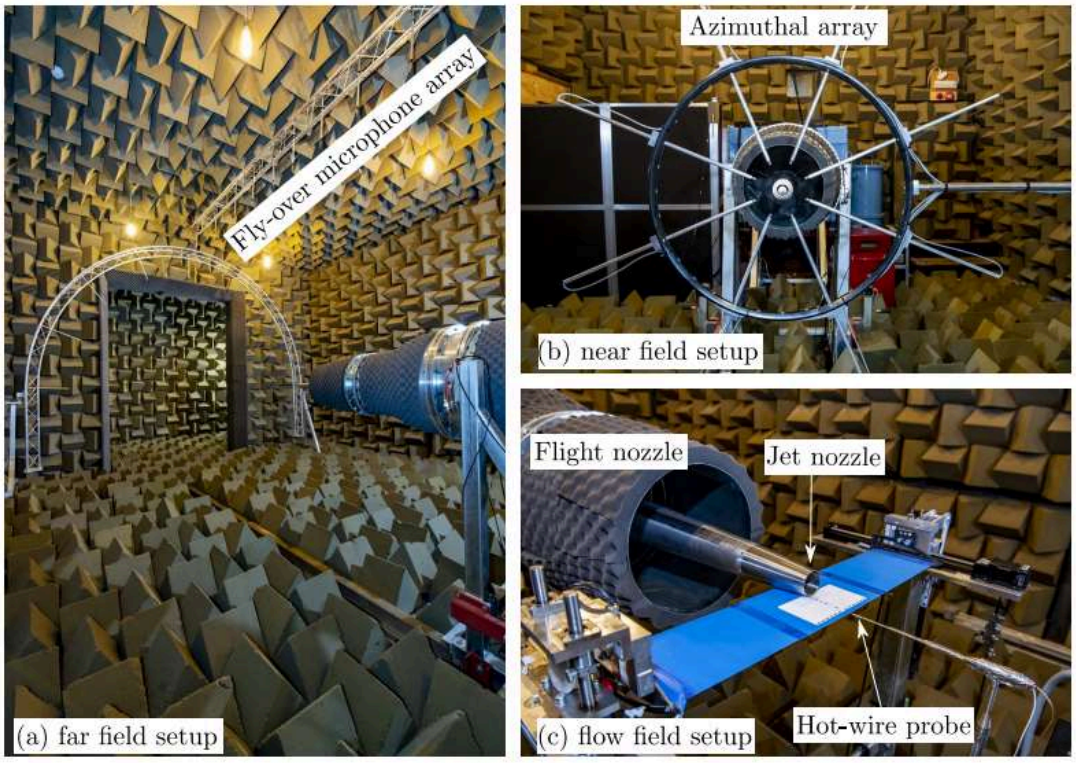

Fig. 1 Photographs of the Flight Jet Rig in the Doak Laboratory at the University of Southampton

Far-field data has been obtained using a linear 'fly-over' microphone array, as indicated in Fig. 1a. Ten 1/4" GRAS Type 40BF condenser microphones, conditioned with B&K Falcon Type 2670 pre-amplifiers were used. The microphones were mounted at observer polar angles ranging from 40° to 130°, at 10° intervals. Far-field acoustic data were collected for 10 seconds at a sampling rate of 200 kHz and high-pass filtered at 20 Hz. These data were then converted to 1-m lossless values assuming spherical spreading and by applying atmospheric attenuation and microphone free-field incidence corrections.

Experimental flow-field data were obtained using hot-wire anemometry. A Dantec constant temperature system was used with both single-wire and cross-wire probes. The probe holder was mounted to a fully-automated three-axes ISEL traverse system. An example of this setup is displayed in Fig.1b. Hot-wire probes were calibrated using a Dantec automatic calibrator in the velocity range 5 m/s $\leq U \leq$ 300 m/s. Flow-field data were sampled at 100 kHz, and the total data acquisition time was 2 seconds.

Scaling of the axial velocity component along the jet centerline is considered next. In previous work by NASA [44] the Particle Image Velocimetry (PIV) data from a wide range of single-stream jet flows has been analysed using the Witze's two-parameter functional form [44] to collapse the centreline velocity distribution.

$$\frac{U}{U_j} = 1 - \exp\left(\frac{\alpha}{1 - x/\beta D_j}\right) \tag{1}$$

where α and β are case-dependent dimensionless parameters for jet spreading rate and potential core length, respectively. Once the similitude parameters are obtained for both Doak jets, their centreline meanflow velocity profiles (Fig. 2a) collapse as a function of the dimensionless coordinate $\left(x/D_j - \beta\right)/(\alpha\beta)$ as shown in Figure 2b. The parameters of nondimensionalization of axial coordinate are given in Table 1 and compared with the Witze parameters of similar NASA SHJAR jets reported in [43]. Interestingly, in comparison with the NASA jets, the Doak jets appear to be distinctly different – the latter jets have a markedly shorter potential core and a significantly faster spreading rate. To understand the difference with the NASA jets, Fig.3 shows velocity spectra measured in several hot-wire locations along the centreline of the Doak jets. For the fast Ma=0.8 jet, the velocity spectrum just downstream of the nozzle exit exhibits multiple discrete tones from $St_D \sim 0.5$ to $St_D \sim 4$. The Ma=0.6 Doak jet shows two relatively weak high-frequency tones at $St_D \sim 1$ and $St_D \sim 4$ downstream of the nozzle exit. The nature of the tones in the velocity spectra is unclear: one cannot rule out the hot-wire interference. The reflection from the hot-wire probes can also affect the trapped modes, which propagate in the jet potential core and reflect from the converging shear layers and the upstream flow condition in the rig [45]. It can be noted that in the case of the Ma=0.8 Doak jet, the prominent tones at frequencies $St_D \sim 0.5$ and $St_D \sim 1$ are similar to the first two dominant peaks in the power spectral density of the pressure in the near-nozzle region of the Mach 0.9 isothermal jet in the study of Towne et al. (e.g. see Fig.10 in [45]).

In the case of the Ma=0.6 Doak jet, there is also a broad hump in the velocity spectrum at the centreline location approximately corresponding to the collapse of the jet shear layers. The hump in the velocity spectrum, bearing the signature of coherent structures in the quasi-laminar jet shear layers, does not exist at the Mach number 0.8 jet. This suggests that the shear layers of the latter faster jet show a more turbulent behaviour compared to the Ma=0.6 jet.

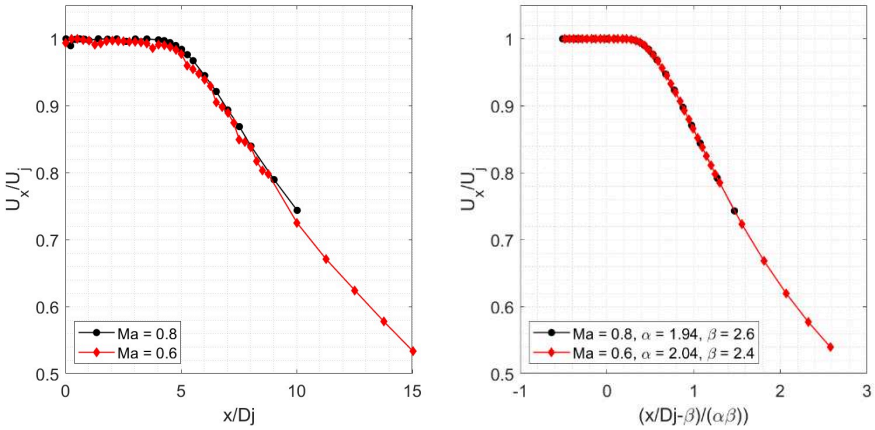

(a) (b)

Fig. 2 Centerline profile of mean velocity for Ma = 0.6 and 0.8 jets (a) and rescaled by the Witze model (b).

Table 1. Jet flows and parameters of nondimensionalization of axial coordinate from the NASA SHJAR jets [43] at different Set Points (SP) **and the Doak experiment.**

Nozzle	Ma	Tj/Ta	α	β
SHJAR SP3	0.5	0.95	0.777	4.47
SHJAR SP5	0.7	0.89	0.656	5.21
SHJAR SP7	0.9	0.84	0.595	6.21
Doak jets	0.6	1.07	2.04	2.4
	0.8	1.05	1.94	2.6

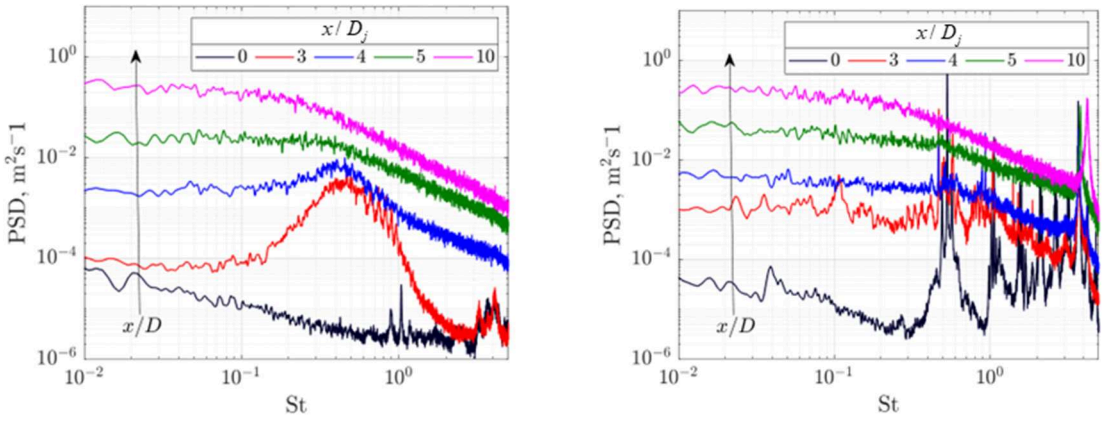

Fig. 3 Power Spectral Density (PSD) of stream-wise velocity fluctuations along the jet centerline for Ma = 0.6 (a) and Ma=0.8 (b).

III.Computational Model Set-Up and Flow Solutions

The computational domain includes a part of the nozzle exhaust and extends for about $100D_j$ downstream of the nozzle exit and $30D_j$ radially. The inlet boundary conditions upstream of the nozzle exit were tailored to mimic profiles of the mean flow velocity and turbulent velocity fluctuations measured downstream of the nozzle exit as closely as possible. This is achieved by imposing the characteristic boundary conditions, which correspond to the prescribed jet Mach number at the nozzle exit. Synthetic turbulent velocity fluctuations were included in the incoming local Riemann invariants following the previous work [34]. In accordance [46], the synthetic turbulent fluctuations were computed using the off-the-shelf synthetic turbulence generator method [47, 48]. The imposed velocity fluctuations satisfy to the von-Karman Pao wavenumber spectrum of the turbulent kinetic energy. Instantaneous realisations of the velocity fluctuations were computed in a box domain, which matches the nozzle inlet geometry. To mimic the effect of turbulence convection by mean flow, the fluctuations were obtained on consecutive slices of the turbulence box separated by a distance in accordance with the local mean flow velocity at the flow inlet. The number of cells and waveforms in each direction of the turbulence box are adjusted so that the generated turbulent structures are sufficiently resolved on the LES grid near the wall. The magnitude of the imposed velocity wavenumber spectrum and the slices of the turbulence box are adjusted so that the resulting root-mean-square (r.m.s.) of axial velocity fluctuations and axial mean flow velocity profile downstream of the nozzle exit agree with the measurements as closely

as possible. Figure 4 displays the mean axial velocity and r.m.s. axial velocity obtained by both experiments and LES at $0.025D_j$ downstream of the jet nozzle exit plane.

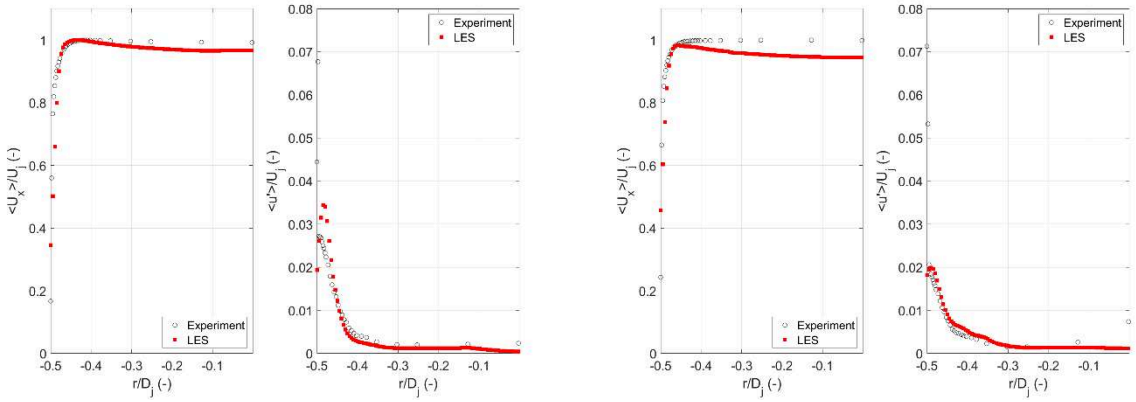

(a) (b)

Fig. 4 Comparison of the solution profiles obtained from LES at a distance of $0.025D_j$ downstream of the nozzle exit with the experiment: mean axial velocity and r.m.s. of axial velocity fluctuations for Ma = 0.6 (a) and Ma = 0.8 (b) jet cases.

For wall modelling, the size and thickness of the grid layers near the boundary can be precisely controlled in the framework of the OpenFOAM snappyHexMesh routine, which involves adding body-fitted hexahedral grid layers near the viscous wall boundary. During the automatic meshing procedure, the distance between the centres of control volumes close to the boundary and the boundary itself are kept within a prescribed value. Following [34, 46] the so-called equilibrium wall model is considered. Inside the boundary layer mesh, the cell centred values of the velocity and density are evaluated at each time step. These values are provided to the wall model, which, in turn, provides the wall shear stress. Consequently, this wall shear stress is used as a boundary condition for the LES at the wall. The wall model is based on the algebraic method using Reichardt's law as described in [49]. Reichardt's law of the wall gives a relation between the local u+ and the y+ of the wall, whereas in the WMLES calculation the instantaneous velocity is used as the input to the wall law. The resulting non-linear algebraic equation for the velocity profile is solved by a simple Newton iteration, giving the wall shear stress at a negligible cost compared to the LES time step.

At the external boundaries, characteristic non-reflecting boundary conditions based on the local Riemann invariants were applied together with grid stretching like in the previous jet flow calculations [34].

Before performing the final simulations, several LES grids were considered and gradually refined in the jet shear layer zone, making use of the fast GPU solution turnaround times. The grid refinement enabled capturing important

small-scale details in the sensitive jet shear layer region, whilst ensuring the final flow and noise solutions are more-or-less insensitive to the grid resolution. The grid refinement aligns with the spreading shear-layer and gradually reduces in the axial direction to optimize the grid density distribution. Images of the LES mesh for the Ma=0.8 Doak jet are shown in Fig.5.

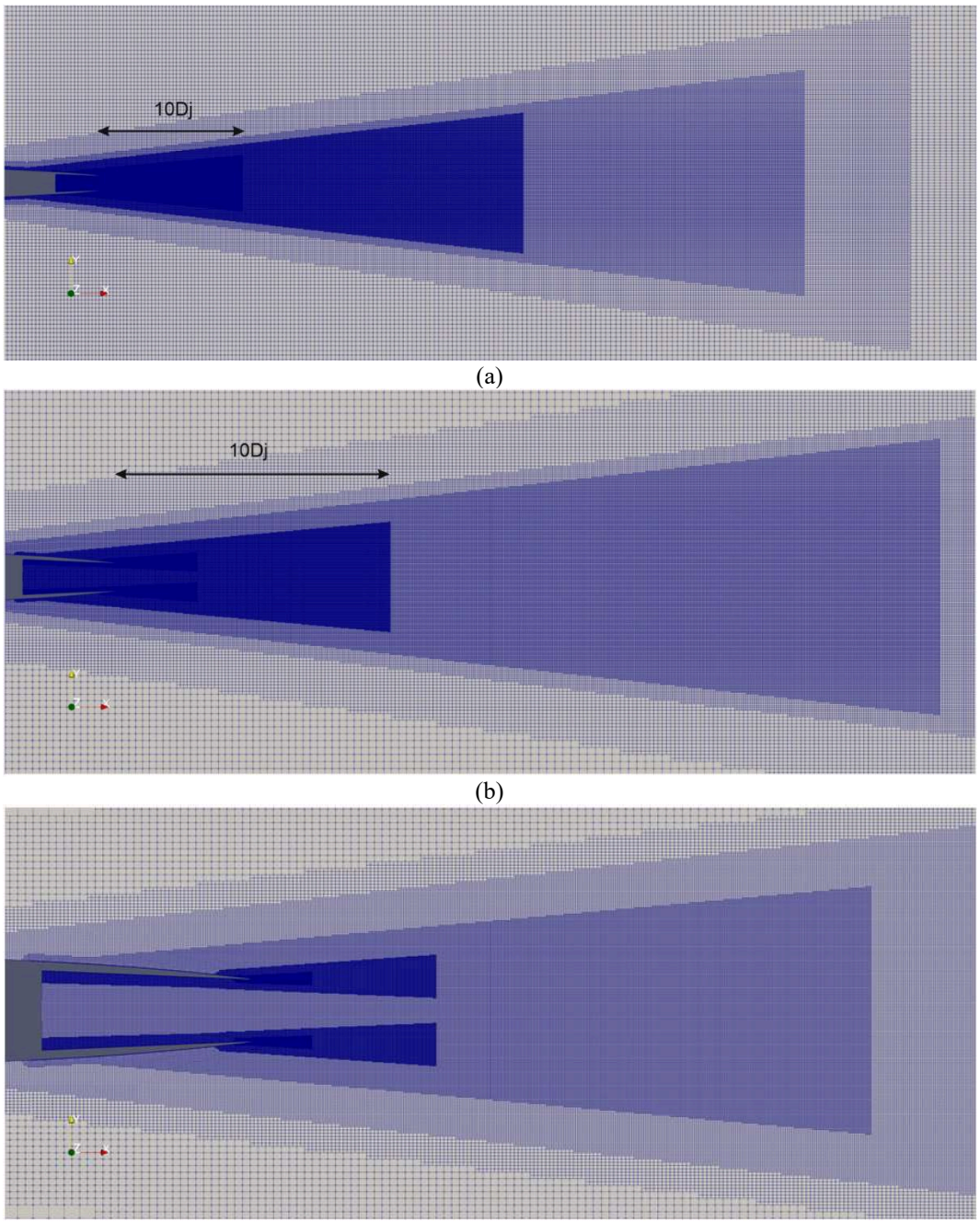

Fig. 5 A series of zoomed-in images of the LES mesh in the jet symmetry plane for the Ma=0.80 case – from (a) to (c). The area of refined mesh inside the nozzle is shown in (c).

In comparison with the Ma = 0.8 jet, the slower Ma = 0.6 jet corresponds to a faster spreading of the shear layers. Hence, the non-uniform LES grid initially generated for the Ma = 0.8 jet case, was further modified to accommodate the thicker initial shear layers of the Ma = 0.6 jet. To achieve this, an additional mesh refinement was applied within a larger radial zone centered around the jet lip-line location in comparison with the original mesh for the Ma = 0.8 jet. In comparison with the latter mesh, the boundary layer grid inside the nozzle and in the early shear layer region of the Ma=0.6 jet case was refined in all directions by a factor of 3. The resulting grid size increase was partly leveraged by simulating a shorter section of the upstream nozzle geometry with imposing appropriate synthetic turbulent inflow boundary conditions closer to the nozzle exit in comparison with the Ma = 0.8 case. In addition, since it is known that the development of jets with relatively broad initial shear layers can be sensitive to the inflow turbulence [24], it was made sure that the turbulence intensity profile downstream of the nozzle exit is particularly well-matched with the experiment (Fig.4b).

Table 2 compares the details of the final LES meshes generated for the two Doak jets with those available for the previous LES models of high-Reynolds-number jets in the literature. It can be noted that current LES grid count is on the high side, and so is the grid density in the early shear layers. The grid resolution increase was needed to closely mimic details on the inflow conditions for the Doak jets, which have relatively thin early shear layers. To speed up the time to solution with the fine LES meshes, the Doak jet cases were run on a workstation with 2x NVIDIA RTX A6000 GPUs. The total number of convective Time Units (TUs) per hour generated by the GPU CABARET algorithm for the Ma = 0.6 and Ma = 0.8 jets were similar despite the factor of 3 difference in the smallest grid cell size between the two cases. One TU corresponds to the time taken for a turbulent eddy moving with the jet speed at the nozzle exit to pass the distance equal to the nozzle diameter. The relatively small computational cost increase for the fine mesh calculation with decreasing the smallest cell size is due to the asynchronous time stepping algorithm implemented in the CABARET method, where the smallest local time step is only used in the finest grid zone, which is a small part of the total jet volume. The asynchronous time-stepping implemented on GPU allowed completing the LES runs within 10-15 days, whilst obtaining a sufficiently long time-signal for statistical analysis. A total of 300 TUs for the initialization run, plus 1000 TUs for statistics, were computed for the Ma = 0.6 case and 300 plus 1100 TUs were computed for the Ma = 0.8 case.

Table 2. Grid resolution details at the jet lip-line location $r / D_j = 0.5$ and total mesh counts for the current Doak flow simulations in comparison with the jet LES literature.

Jet Case	Ma	Mesh resolution						Total mesh count
		dx/D_j		dr/D_j		$rd\theta/D_j$		
		Nozzle lip	Potential core	Nozzle lip	Potential core	Nozzle lip	Potential core	
Doak	0.6	0.00375	0.0150	7.5e-4	0.0125	0.003125	0.0125	196mln
	0.8			1.5e-3				135mln
Doak [24]	0.6	0.0125	0.02	0.0017	0.005	-	-	-
PPRIME [22]	0.9	0.0030	-	0.0034	-	0.0030	-	10.8mln
		0.0015	-	0.0017	-	0.0015	-	64.2mln
SILOET [31]	0.9	0.00640	0.0167	4.92e-4	0.0122	0.0061	0.0123	90mln
SHJAR [32]	0.5 0.9	0.010	0.0122	7.87e-4	0.0089	0.0089	0.0089	101mln

Figures 6-9 show the comparison of the LES solution with the experimental data. Radial profiles of the axial mean flow velocity and axial velocity fluctuations are shown for the $\mathrm{Ma} = 0.6$ and $\mathrm{Ma} = 0.8$ jet cases. For the $\mathrm{Ma} = 0.6$ case, an overall good agreement is obtained for both the mean flow velocity distributions and the turbulent velocity fluctuations. Some discrepancies are noticeable close to the jet centreline, where the LES underpredicts the turbulent mixing compared to the experiment, as well as at further downstream locations of the jet, where the LES tends to overpredict the potential core length. The comparison between the LES results and the experiment for the $\mathrm{Ma} = 0.8$ jet follows the same trends as for the $\mathrm{Ma} = 0.6$ case apart from larger discrepancies around the jet centreline. As a series of numerical tests on different LES grids have confirmed, the noted discrepancies with the hot-wire measurements near the centreline are virtually insensitive to the LES grid resolution.

Similar to the previous discussion of the differences between the Doak Laboratory and NASA SHJAR datasets, two working hypotheses are suggested to explain the discrepancies between the LES and the hot-wire measurements.

Firstly, the intrusive measurement procedure used in the Doak Lab experiment, where the probes immersed in the flow trigger additional jet mixing, and which effect was not present either in the LES model or the SHJAR PIV tests. For example, the effect of probe vibration may be particularly noticeable inside the potential core of the jet at Mach number 0.8 where the strong tones are observed in the velocity spectrum (see Figure 3b). Additionally, the hot-wire measures the resultant instantaneous momentum flux perpendicular to the wire element, which may not be straightforwardly related to the turbulent velocity fluctuations extracted from the current LES, which did not consider the hot wire probe.

The second hypothesis considers the difference in the upstream boundary conditions between the LES and the Doak experiment. The Doak Laboratory's FJR has a constant 2.4° convergence pipework extending 19 jet diameters upstream of the nozzle exit. This long convergent nozzle creates a small vena contract effect and a very thin boundary layer at Mach numbers 0.6 and 0.8, which is expected to be fully turbulent at the nozzle exit. Simulation of the entire upstream wind-tunnel section with LES would be unfeasible. Hence, the LES solution was started at some distance upstream of the nozzle exit, whilst capturing the same mean flow velocity and turbulence intensity profiles for the stream-wise velocity component at $0.025\,D_j$ downstream of the nozzle exit as in the Doak experiment. No attempt was made to incorporate in the LES model either the information about the other two fluctuating velocity components, or the space-time correlations downstream of the nozzle exit. No such information was available from the Doak experiment. At the same time, for example, for initially laminar high-speed jet flows, it is well-known that prescribing just the mean flow and turbulent intensity profiles is not sufficient to fully determine the jet flow development downstream of the nozzle exit especially in relation to the properties pertinent for jet noise generation such as the auto-covariance of fluctuating turbulent stresses [10, 50].

As discussed in the next sections, it is possible to further shed light on the origin of the discrepancies between the Doak experiment and the LES jet flow solutions by comparing the far-field noise datasets, where the effect of the hot-wire probe interference is ruled out because the probes were removed from the flow for acoustic measurements.

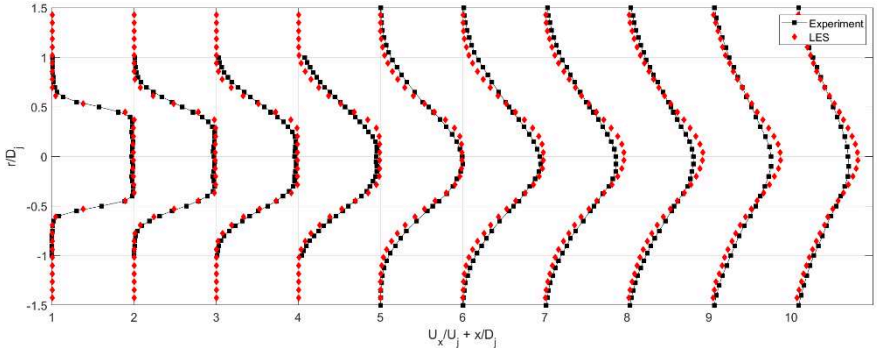

Fig. 6 Radial profiles of mean axial velocity compared to experimental results for the Ma=0.6 case.

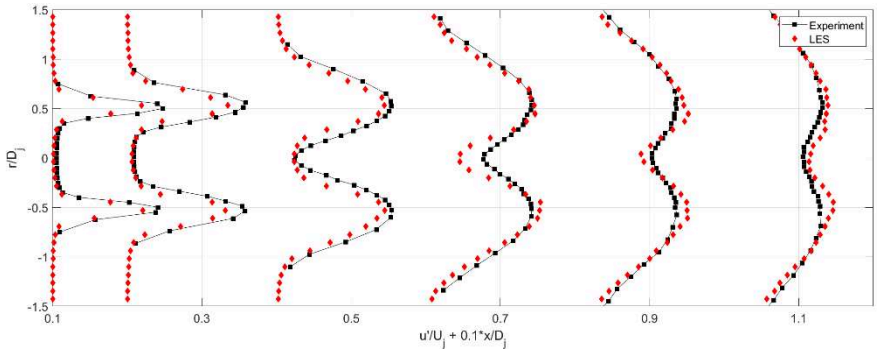

Fig. 7 Radial profiles of the r.m.s. fluctuations of axial velocity compared to experimental results for the Ma=0.6 case

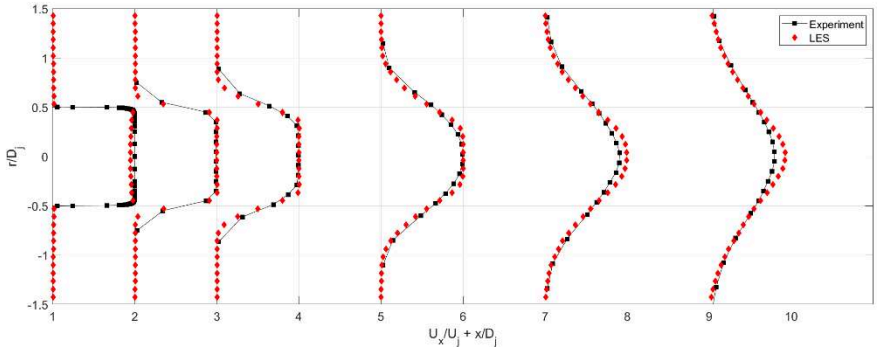

Fig. 8 Radial profiles of mean axial velocity compared to experimental results for the Ma=0.8 case.

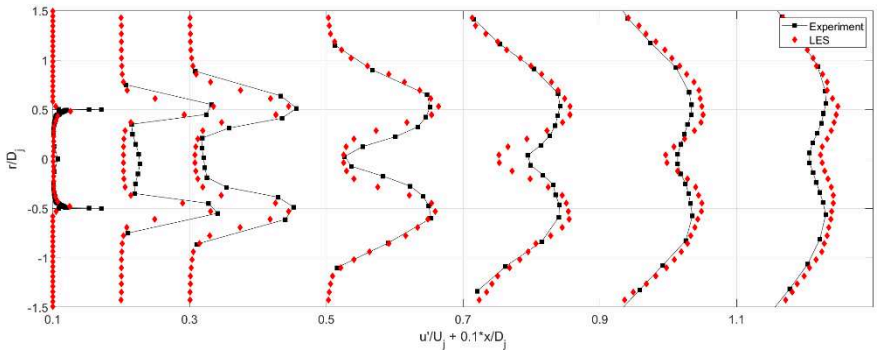

Fig. 9 Radial profiles of the r.m.s. fluctuations of axial velocity compared to experimental results for the Ma=0.8 case.

IV.Acoustic Models, Far-Field Noise Results, and Discussion

The first method considered for far-field noise calculations is based on the penetrable-surface formulation of the time-domain Ffowcs Williams-Hawkings (FW-H) method [27]. FW-H is a general Computational Aero-Acoustics method, as it uses the complete space-time LES flow fields on acoustic control surfaces, which are appropriately set up to confine most important jet noise sources in the jet flow. In particular, following the previous experience with static single-stream jet noise calculations with GPU CABARET [32, 33], a conical acoustic control surface (Fig.10) was used with 16 closing discs [6] placed at 35 to 45 nozzle diameters downstream of the nozzle exit. For computing the spectra of the time pressure signal, the standard Welch method of Fourier transforms of short periodograms was used, the implementation details for which can be found in [34]. The FW-H acoustic integration surfaces were set up so that their grid resolution near the nozzle exit corresponds to the maximum resolved Strouhal number of $St_D = 11$, based on 8 PPW (Points Per acoustic Wavelengths), and $St_D = 2$ near the end of the acoustic surface.

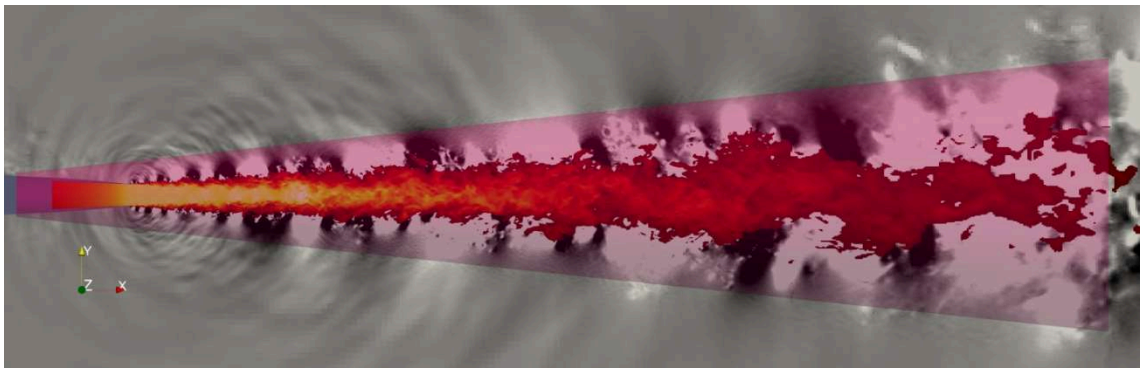

Fig. 10 The instantaneous velocity contours (scale 0 to 310 m/s) and the pressure waves (scale -100Pa to 100Pa from ambient, p_0). The jet volume inside the FW-H surface is highlighted.

In addition to the FW-H method, far-field noise spectra of the Doak jets are calculated using the reduced-order implementation of the Goldstein Generalised Acoustic Analogy (GAA) [37-39]. In the current implementation, following [36, 37], the time-averaged LES solutions in the jet symmetry plane are used to statistically model the effect of noise generated by fluctuating Reynolds stresses in the jet shear layers. In comparison with the FW-H method, the GAA model can take RANS-type mean flow and turbulence solution components as an input, thereby is suitable for quick turnaround-time noise calculations on a personal laptop, whilst still producing physical insights into effective sources of jet noise. The reduced-order model uses several dimensionless proportionality coefficients to compute the

correlation length scales and amplitudes from the local mean flow and turbulence quantities. The proportionality coefficients of the GAA model for the Doak jets are assumed to be the same as previously obtained for several other high-speed jet cases including SILOET and NASA SHJAR SP3 and SP7 [36, 37]. Details of the GAA model implementation are provided in Appendix A.

The third jet noise method considered is the purely empirical NASA sJet model [35], which is based on interpolations across a large number of NASA SHJAR jet cases using scaling laws. Essentially, the sJet model provides the far-field noise spectra equivalent of the NASA SHJAR jets for the same nozzle pressure and temperature conditions as in the Doak experiment.

Figure 11 shows the comparison of the far-field noise spectra results of the LES-FW-H method with the Doak Laboratory experiment data and the sJet predictions for the Ma = 0.6 jet for a range of polar observer angles relative to the downstream jet axis. At 30°, no experimental data are available, hence, the LES results are compared only to the sJet solution. Figure 12 shows the same comparison for the Ma = 0.8 jet.

For the slower Ma = 0.6 jet, the LES solutions are within 1-2 dB of the experimental data for frequencies ranging from $St_D = 0.04$ to $St_D = 10$ for observer angles from 30 to 70 degrees. For large observer angles, 80-100° a moderate 2-3dB hump develops in the noise spectra of the LES solution at Strouhal numbers 6-7. This hump is likely to be associated with an insufficiently extensive region of the LES grid refinement in the radial direction of the Ma=0.6 jet close to the nozzle exit, where the early shear layers are thicker compared to the Ma=0.8 jet case, for which the high-frequency hump is not observed. The sJet predicts 1-2 dB more noise compared the Doak Laboratory data for high observer angles at high frequencies and for the peak jet noise frequencies at the 40° observer angle to the jet flow. For this jet case, the LES results are closer to the sJet dataset showing a discrepancy with the latter of 1-2 dB for a wide range of frequencies $0.04 < St_D < 10$ over a range of observer angles, from 30° to 90°. Furthermore, the peak noise predictions of the LES model at 30-40° angles agree with the sJet dataset within 0.5-1dB. The above suggests that the difference between the Doak experiment data and the LES model for the Ma=0.6 jet is likely to be associated with differences in the jet inflow condition beyond the mean flow and turbulence intensity distributions, such as due to anisotropy. Recalling the previous discussion of the quasi-laminar behaviour of the velocity spectrum of the Ma=0.6 Doak jet (Fig.3a), it can be hypothesised that the observed high sensitivity to the inflow condition is associated with a not-fully turbulent state of the shear layers in this slower jet case.

For the faster Ma = 0.8 jet, for most oberver angles, the LES-FW-H results are within 1 dB of the Doak experimental data from $St_D = 0.04$ to $St_D = 7$ and within 2 dB up to $St_D = 8$. For this jet case, the sJet solutions are also in excellent agreement (within 0.5-1dB) with the Doak dataset including the peak noise frequencies. Some discrepancies only appear at very high frequencies St_D = 8-10, where the Doak Laboratory jets show 1-2dB more noise compared to the equivalent NASA SHJAR jets. Hence, for the M=0.8 jet case, all three datasets, the Doak measurements, the LES-FW-H predictions, and the equivalent NASA SHJAR data show a much better agreement compared to the Ma=0.6 case.

This suggests that the previously reported differences between the mean flow solution for the Ma=0.8 jet case and the hot-wire measurements related to the prominent discrete tones in the velocity spectrum (Fig.4b), were caused by the hot-wire probe interference effect. For this faster jet case, which does not show a hump in the velocity spectra typical of the quasi-laminar shear layers, the LES inflow boundary conditions based on replicating the experimental profiles of the mean flow velocity and turbulence intensity downstream of the nozzle exit appear to be sufficient to accurately reproduce the noise generation mechanisms.

Finally, Figs. 13 and 14 compare the predictions of the reduced-order model based on the GAA model with the Doak Laboratory experimental data and the sJet predictions. Overall, noise spectra predictions of the GAA model are within 2-3dB agreement with the Doak Laboratory dataset for most frequencies from $St_D = 0.04$ to $St_D = 4$ and observer polar angles from 30 to 90 degrees. There are some discrepancies with the experiment at the higher frequencies, where the current GAA solutions tend to overpredict the rate the noise spectra roll-off. In addition, the model shows some 3-4dB noise amplification for the upstream observer angle. These discrepancies suggest that the Doak jets are different from the SILOET and NASA jets, for which the original GAA model was calibrated, thereby suggesting that the dimensionless proportionality coefficients of the reduced-order acoustic model need to be specifically adjusted for the Doak jets.

Nevertheless, despite its simplicity, the current implementation of the GAA model does capture a difference between the Doak Ma=0.6 and 0.8 jets. Indeed, for the Ma = 0.6 jet, the GAA model underpredicts peak noise in comparison with the Doak measurements by 1-2dB at the 40^o observer angle, which lies within the uncertainty between the Doak and the sJet datasets. In comparison with this, for the Ma = 0.8 jet case, the noise prediction of the GAA model close to the peak jet nose direction is within 1dB from the Doak Laboratory measurements. Again,

this suggests that, compared to the Ma=0.6 Doak jet, the Ma=0.8 jet is more similar to NASA SHJAR jet flows, which do not exhibit a quasi-laminar shear layer behaviour and high sensitivity to fine details of the upstream rig condition.

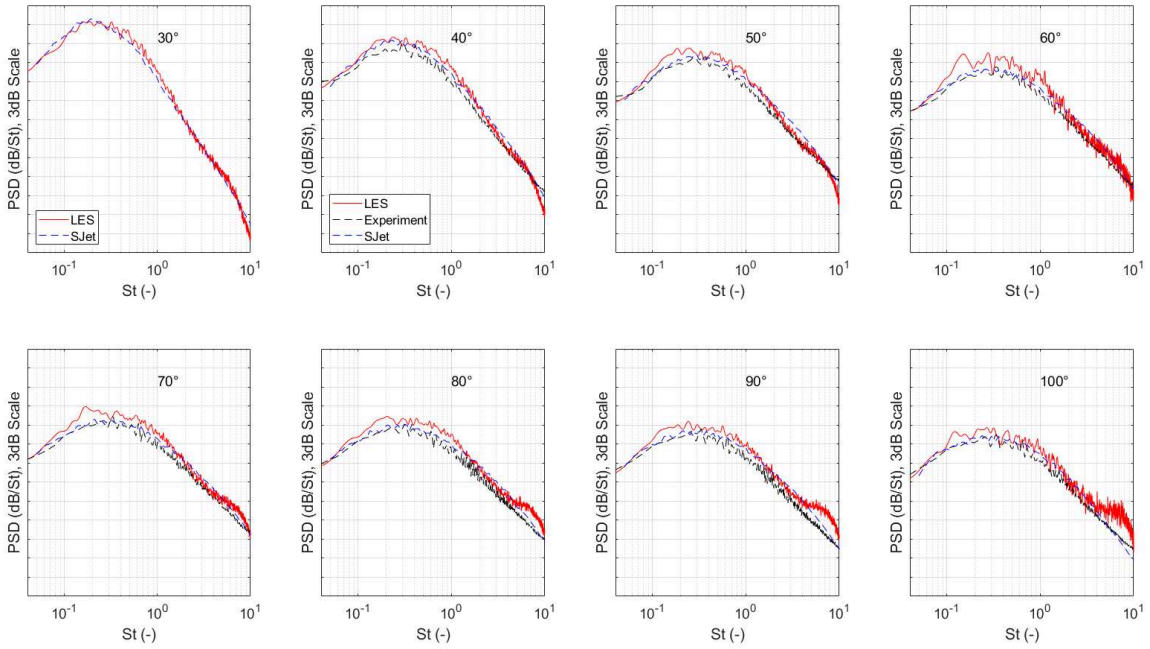

Fig. 11 Comparison of far-field noise predictions of the LES FW-H method for the Ma = 0.6 jet with the Doak measurements and sJet data at eight polar observer angles. The LES results correspond to the statistical averaging over 1000 convective time units.

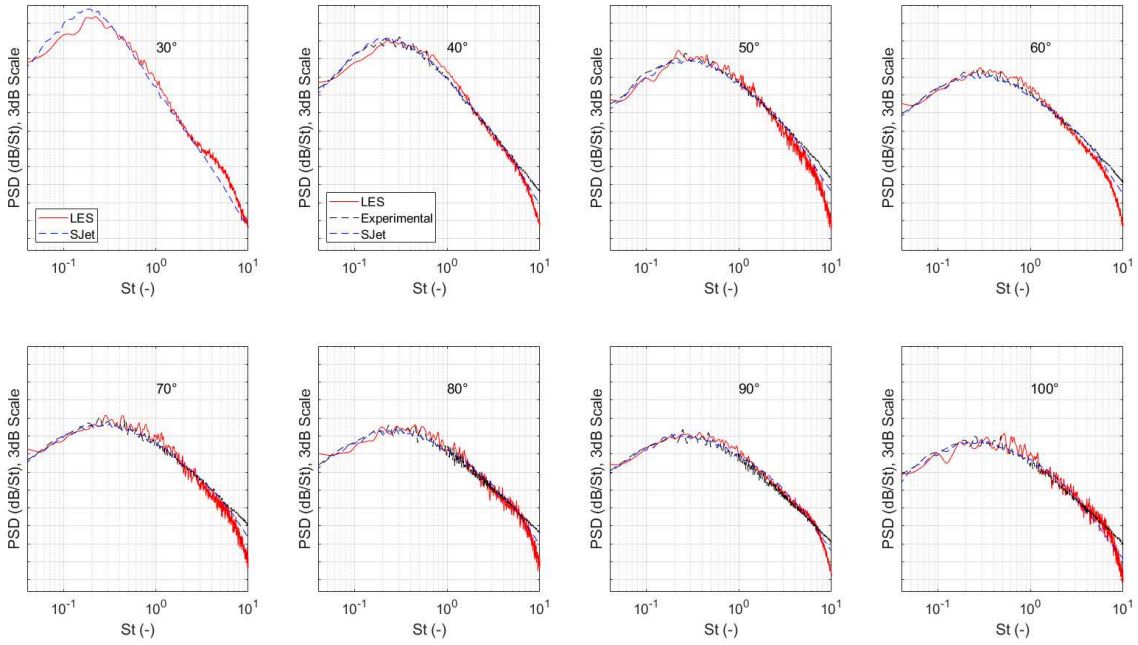

Fig. 12 Comparison of far-field noise predictions of the LES FW-H method for the Ma = 0.8 jet with the Doak measurements and sJet data at eight polar observer angles. The LES results correspond to the statistical averaging over 1100 convective time units.

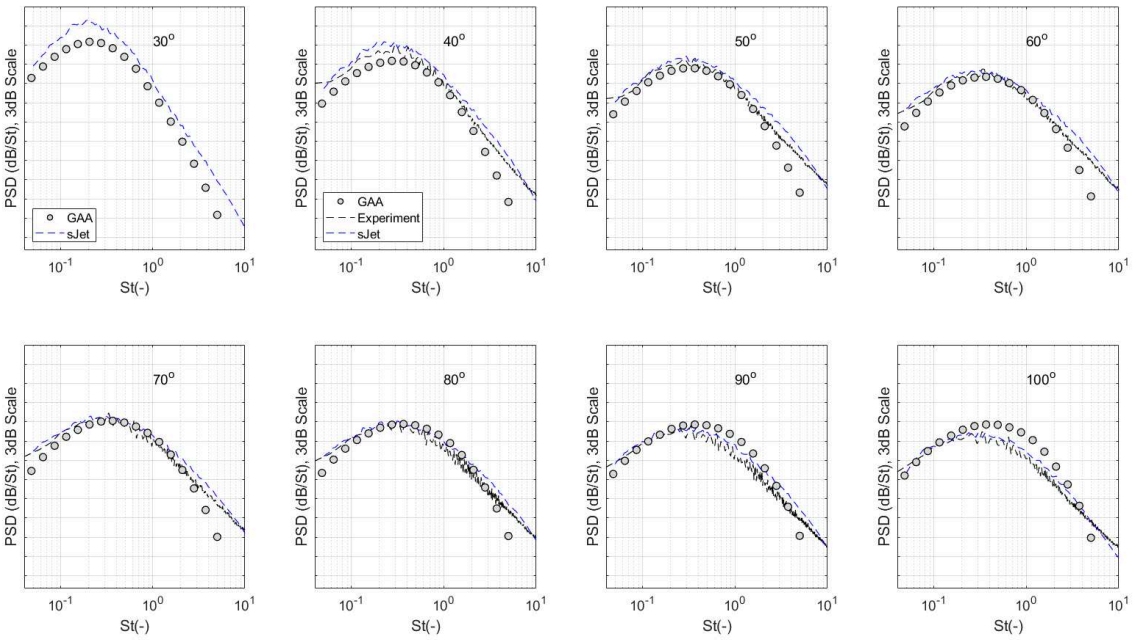

Fig. 13 Comparison of far-field noise predictions of the reduced-order GAA model for the Ma = 0.6 jet with the Doak measurements and sJet data at eight polar observer angles.

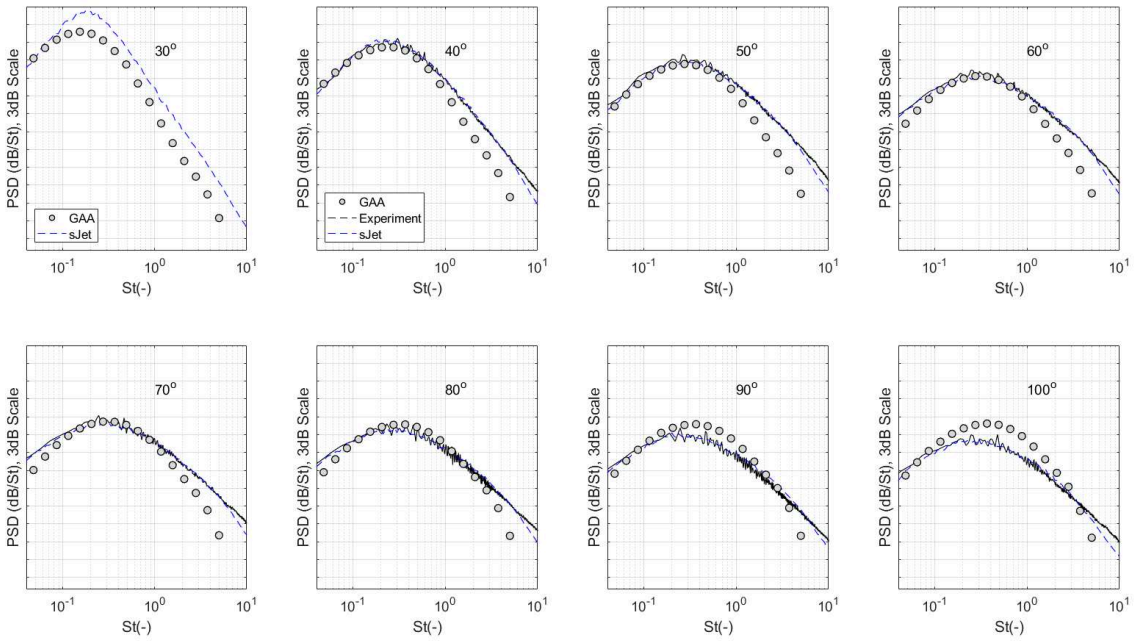

Fig. 14 Comparison of far-field noise predictions of the reduced-order GAA model for the Ma = 0.8 jet with the Doak measurements and sJet data at eight polar observer angles.

V.Conclusions

Flow and noise solutions obtained from the Wall Modeled Large Eddy Simulations (WMLES) of the Mach 0.6 and Mach 0.8 jets of the Doak Laboratory Flight Jet Rig experiment have been performed and critically analyzed in comparison with the NASA SHJAR dataset. The WMLES calculations were based on the high-resolution CABARET method accelerated on GPU. The achieved acceleration allowed to perform simulation runs for 1300-1400 convective time units on 135-196 million LES meshes, which are sufficiently well-resolved in the region of the initial thin shear layers to mimic the mean flow and turbulence intensity profiles measured in the Doak experiment just downstream of the nozzle exit.

It is shown that the Witze parameters of the mean flow velocity profiles of the Doak jets, such as the potential core length and the jet spreading rate are significantly different from the NASA SHJAR SP3, SP5, and SP7 jets corresponding to the same range of Mach and Reynolds numbers. In addition, the hot-wire measurements show that the velocity spectrum of the Ma=0.6 jet exhibits a hump typical of quasi-laminar shear layers, while the velocity spectra of the Ma=0.8 jet show notable discrete tones for the probe location close to the nozzle exit. The LES solutions

show a better agreement with the hot-wire measurements for the Ma=0.6 jet compared to the Ma=0.8 jet case, where larger discrepancies around the jet centreline are noted for turbulent velocity fluctuation profiles. Possible reasons for the discrepancies between the Doak measurements and the Witze parameters extracted from the NASA SHJAR PIV data, as well as between the Doak dataset and the LES solutions, are due to differences in the upstream rig conditions, not accounted for in the mean flow and turbulence intensity profiles, and the hot-wire probe interference with the jet flow.

These differences are further analyzed by comparing the far-field noise spectra corresponding to the acoustic measurements in the Doak Laboratory, the solutions of the LES method coupled with the state-of-the-art Ffowcs Williams and Hawkings (FW-H) method, and the solutions of the empirical sJet model, which represents interpolations across the NASA SHJAR jet noise database for the Doak jet conditions. The far-field noise comparisons allow to separate the hot-wire probe interference effect, since the acoustic measurements in the Doak Laboratory were performed with removing the hot-wire probs from the flow. In addition, noise spectra predictions for the same Doak jets are also computed by implementing a reduced-order version of the Goldstein Generalized Acoustic Analogy (GAA) model, which uses the local mean flow and turbulence data from the LES solutions of the Doak jets along with the dimensionless space, time, and amplitude parameters of the auto-covariance function from the literature.

For the Ma=0.6 jet, it is shown that the noise spectra solutions of the LES-FW-H method are within 1-2dB from the sJet predictions and 2-3dB from the Doak noise measurements. There is also a 1-2dB discrepancy between the sJet solutions and the Doak dataset, which includes the 40^o angle close to the peak jet noise direction. The GAA model, which uses the dimensionless parameters of the effective acoustic source obtained from other turbulent jet cases, also shows a similar 1-2 dB uncertainty of the peak noise predictions in comparison with the Doak experiment. These suggest that the noise spectra of the Ma=0.6 jet are quite sensitive to the upstream conditions in-line with the quasi-laminar behavior of the velocity spectrum in the hot-wire measurements. In this case, imposing just the low-order statistics such as mean flow velocity and turbulent intensity profiles downstream of the nozzle exit appears to be insufficient to accurately determine acoustic properties of the jet flow.

For the Ma=0.8 jet, peak noise predictions of the LES-FW-H, sJet, and GAA models at the 40^o observer angle agree with Doak measurements within 1dB. Furthermore, the LES-FW-H noise spectra solutions, sJet, and the Doak experiment are within 1dB for most observer angles up to a frequency of $St_D = 7$. Collectively, this suggests that the strong tones observed in the velocity spectra of the hot-wire measurements in this jet flow were most likely due to

the hot-wire probe interference effects. Once the probes are removed from the flow, the Doak jet shows a similar behavior to other high-speed single-stream jets in the literature such as NASA SHJAR. In this case, setting up the inflow boundary conditions in LES to more-or-less accurately match the mean flow velocity and turbulence intensity profiles of the experiment is sufficient for accurate noise predictions.

Appendix A. Reduced-Order Implementation of the Generalized Acoustic Analogy Model

In accordance with the Generalized Acoustic Analogy (GAA) model [39], the power spectral density of the far-field pressure signal can be expressed as the following convolution integral of the source term with the propagator function:

$$S(\mathbf{x},\omega)=\int_V\int_V \hat{R}_{ijkl}(\mathbf{y},\boldsymbol{\Delta},\omega)\hat{I}_{ij}(\mathbf{y},\omega;\mathbf{x})\hat{I}^*_{kl}(\mathbf{y}+\boldsymbol{\Delta},\omega;\mathbf{x})d\boldsymbol{\Delta}d\mathbf{y}, \tag{A1}$$

where $\mathbf{x}$ and $\mathbf{y}$ are observer and source coordinates, respectively, $\boldsymbol{\Delta}$ is the space separation vector in the source coordinates, ω is angular frequency, and $\hat{\cdot}$ denotes to the Fourier transforms.

In particular, $\hat{R}_{ijkl}(\mathbf{y},\boldsymbol{\Delta},\omega)$ is the Fourier transform of the generalised Reynolds stress tensor auto-covariance term, so that

$$\hat{R}_{ijkl}(\mathbf{y},\boldsymbol{\Delta},\omega)=\int_{-\infty}^{\infty} R_{ijkl}(\mathbf{y},\boldsymbol{\Delta},\tau)e^{i\omega\tau}d\tau, \text{ where } R_{ijkl}(\mathbf{y},\boldsymbol{\Delta},\tau)=\overline{T'_{ij}(\mathbf{y},t)T'_{kl}(\mathbf{y}+\Delta,t+\tau)}, \tag{A2}$$

the overbars stand for averaging over time t and $i,j,k,l=1,2,3$, where the corresponding stress term is defined as

$$T'_{ij}=\left(\rho v'_i v'_j-\overline{\rho}\widetilde{v'_j v'_j}\right),\ i,j,k,l=1,2,3 \tag{A3}$$

where v'_i is the fluctuating velocity component, ρ is the density, and the tilde stands for Favre-averaging.

The components of the second-rank wave-propagation tensor of the sound integral (A1) are defined by

$$\hat{I}_{ij}(\mathbf{y},\omega\,|\,\mathbf{x})=\frac{\partial\hat{v}_j^{(a)}(\mathbf{y},\omega\,|\,\mathbf{x})}{\partial y_i}-\left[\frac{\partial\tilde{v}_j}{\partial y_i}(\mathbf{y})\hat{p}^{(a)}(\mathbf{y},\omega\,|\,\mathbf{x})+\tilde{v}_j\frac{\partial\hat{p}^{(a)}(\mathbf{y},\omega\,|\,\mathbf{x})}{\partial y_i}\right]$$
$$+\frac{\delta_{ij}}{2}\left(i\omega+\tilde{v}_k\frac{\partial}{\partial y_k}\right)\hat{p}^{(a)}(\mathbf{y},\omega\,|\,\mathbf{x}), \tag{A4}$$

where $\hat{v}_j^{(a)}$, $\hat{p}^{(a)}$ are components of the Fourier transforms of the adjoint Green's function of the GAA [38].

The adjoint vector Green's function is obtained by solving the locally parallel flow equations with the coefficients defined from the LES mean flow solution, the details for which can be found in [36, 41, 51].

A simple exponential-Gaussian model is used following the works of [35, 40, 52]

$$R_{ijkl}(\mathbf{y},\boldsymbol{\Delta},\tau) = A_{ijkl}(\mathbf{y})\exp\left[-\frac{|\Delta_1|}{\tilde{v}_1\tau_s} - \frac{\ln 2}{l_s^2}\left((\Delta_1 - \tilde{v}_1\tau)^2 + \Delta_2^2 + \Delta_3^2\right)\right] \tag{A5}$$

where τ_s and l_s are the acoustic time and space correlation length scales, which are computed from the turbulent kinetic energy and the mean flow absolute vorticity [36].

$$l_s = c_\ell\sqrt{\kappa}/\xi,\ \tau_s = c_\tau/\xi,. \tag{A12}$$

Following the derivations in [36, 41], assuming the compact source and locally parallel flow approximations are valid, the final noise spectra prediction formula becomes

$$S(\mathbf{x},\omega) = \int_V A_{ijkl}(\mathbf{y})W(\mathbf{y})\hat{I}_{ij}\hat{I}_{kl}^* d\mathbf{y}, \tag{A6}$$

where the function $W(\mathbf{y})$, which emerges as a result of the analytical integration over the correlation volume Δ, is:

$$W(\mathbf{y}) = \left(\frac{\pi}{\ln 2}\right)^{3/2} \frac{2l_s^3\tau_s}{1+(\omega(1-\tilde{v}_1/c_\infty\cos\varphi)\tau_s)^2}\exp\left(-\frac{(\omega l_s/\tilde{v}_1)^2}{4\ln 2}\right). \tag{A7}$$

where, and φ is the observer angle, $c_\infty$is the ambient speed of sound and $\tilde{v}_1$ is the local axial jet mean flow velocity, assumed to be equal to the eddy convection speed, and the amplitudes of the fluctuating momentum source term are modelled using the turbulent kinetic energy, κ,

$$A_{ijkl} = C_{ijkl}(2\bar{\rho}\kappa)^2 \tag{A8}$$

The dimensionless coefficients C_{ijkl}, $i,j,k,l = 1,2,3$ are cylindrical-polar coordinate indices (e_1 is in the jet direction, $e_2 = e_r, e_3 = e_\theta$) were computed from the LES solution along the jet lip-line $r/D_j = 0.5$ in [36]. These

dimensionless amplitude parameters of the major source components are provided in Table A1, which were found to be more-or-less insensitive to the jet case.

Table A1. Amplitude parameters of the GAA model for the fluctuating momentum source term [36]

C_{ijkl}	11,11	rr,rr	$\theta\theta,\theta\theta$	$1r,1r$; $1r,r1$; $r1,1r$; $r1,r1$;	$1\theta,1\theta$; $1\theta,\theta1$; $\theta1,1\theta$; $\theta1,\theta1$	$r\theta,r\theta$; $\theta r,r\theta$; $\theta r,\theta r$; $r\theta,\theta r$
Cold SILOET jet	1	0.355	0.360	0.327	0.326	0.180

The turbulent kinetic energy, mean flow vorticity, mean flow velocity, and other components of the acoustic analogy model are obtained from averaging the LES flow fields. In [36], the dimensionless parameters, $c_l = 2.190$ and $c_\tau = 1.965$ were determined by best fit to the far-field noise data of the SILOET jet at a 90° observer angle. These parameters were also shown to be suitable for acoustic modelling of the NASA SHJAR SP3 and SP7 jets in [36, 37]. Hence, the same parameters are used for acoustic modelling of the $\mathrm{Ma} = 0.6$ and $\mathrm{Ma} = 0.8$ Doak jets.

Acknowledgments

This work is supported by the European Union's H2020 program under the DJINN (Decrease Jet INstallation Noise) project, Grant Agreement No. 861438.

S.A. Karabasov acknowledges the study performed in TsAGI with the financial support provided by the Ministry of Science and Higher Education of the Russian Federation (GrantAgreement of December 8, 2020, No 075-11-2020-023) within the program for creation and development of the World-Class Research Center "Supersonic".

The authors thank Dr Abbas Khavaran for making his sJet code readily available.

Reference List

[1] Tanna, H. K. An Experimental Study of Jet Noise Part I: Turbulent Mixing Noise. Journal of Sound and Vibration, Elsevier BV, 50, 3, Feb, 1977, pp. 405–428. https://doi.org/10.1016/0022-460X(77)90493-X

[2] Bridges, J., and Wernet, M. P. The NASA Subsonic Jet Particle Image Velocimetry (PIV) Dataset. http://rgdoi.net/10.13140/RG.2.1.2844.2485.

[3] Lawrence, J., and Self, R. H. Installed Jet-Flap Impingement Tonal Noise. 21st AIAA/CEAS Aeroacoustics Conference, American Institute of Aeronautics and Astronautics, Jun 18, 2015. https://doi.org/10.2514/6.2015-3118

[4] Proença, A., Lawrence, J., and Self, R. Measurements of the Single-Point and Joint Turbulence Statistics of High Subsonic Jets Using Hot-Wire Anemometry. Experiments in Fluids, Springer Science and Business Media LLC, 60, 4, Mar 13, 2019. 10.1007/s00348-019-2716-3

[5] Proença, A. R., Lawrence, J. L. T., and Self, R. H. Experimental Investigation into the Turbulence Flowfield of In-Flight Round Jets. AIAA Journal, American Institute of Aeronautics and Astronautics (AIAA), 58, 8, Aug, 2020, pp. 3339–3350. https://doi.org/10.2514/1.J059035

[6] Shur, M. L., Spalart, P. R., and Strelets, M. Kh. Noise Prediction for Increasingly Complex Jets. Part I: Methods and Tests. International Journal of Aeroacoustics, SAGE Publications, 4, 3, Jul, 2005, pp. 213–245. https://doi.org/10.1260/1475472054771376

[7] Bodony, D. J., and Lele, S. K. Current Status of Jet Noise Predictions Using Large-Eddy Simulation. AIAA Journal, American Institute of Aeronautics and Astronautics (AIAA), 46, 2, Feb, 2008, pp. 364–380. https://doi.org/10.2514/1.24475

[8] Bogey, C., Marsden, O., and Bailly, C. Large-Eddy Simulation of the Flow and Acoustic Fields of a Reynolds Number 105 Subsonic Jet with Tripped Exit Boundary Layers. Physics of Fluids, AIP Publishing, 23, 3, Mar, 2011, p. 035104. https://doi.org/10.1063/1.3555634

[9] Faranosov, G. A., Goloviznin, V. M., Karabasov, S. A., Kondakov, V. G., Kopiev, V. F., and Zaitsev, M. A. CABARET Method on Unstructured Hexahedral Grids for Jet Noise Computation. Computers & Fluids, Elsevier BV, 88, Dec, 2013, pp. 165–179. https://doi.org/10.1016/j.compfluid.2013.08.011

[10] Bogey, C., and Bailly, C. Influence of Nozzle-Exit Boundary-Layer Conditions on the Flow and Acoustic Fields of Initially Laminar Jets. Journal of Fluid Mechanics, Cambridge University Press (CUP), 663, Nov 04, 2010, pp. 507–538. https://doi.org/10.1017/S0022112010003605

[11] Bogey, C., Marsden, O., and Bailly, C. Influence of Initial Turbulence Level on the Flow and Sound Fields of a Subsonic Jet at a Diameter-Based Reynolds Number of 10^5. Journal of Fluid Mechanics, Cambridge University Press (CUP), 701, May 18, 2012, pp. 352–385. https://doi.org/10.1017/jfm.2012.162

[12] Bridges, J., and Brown, C. Validation of the Small Hot Jet Acoustic Rig for Aeroacoustic Research. 11th AIAA/CEAS Aeroacoustics Conference, American Institute of Aeronautics and Astronautics, May 23, 2005. 10.2514/6.2005-2846

[13] Brown, C. A., and Bridges, J.,Small Hot Jet Acoustic Rig Validation, NASA/TM–2006–214234, 2006.

[14] Angelino, M., Xia, H., Moratilla-Vega, M., and Page, G. Far-Field Noise Prediction of Round and Serrated Jets with Increasingly Refined Grids. 22nd AIAA/CEAS Aeroacoustics Conference, American Institute of Aeronautics and Astronautics, May 27, 2016. https://doi.org/10.2514/6.2016-3047

[15] Ingraham, D., and Bridges, J. E. Validating a Monotonically-Integrated Large Eddy Simulation Code for Subsonic Jet Acoustics. 55th AIAA Aerospace Sciences Meeting, American Institute of Aeronautics and Astronautics, Jan 05, 2017. https://doi.org/10.2514/6.2017-0456

[16] Leib, S. J., Ingraham, D., and Bridges, J. E. Evaluating Source Terms of the Generalized Acoustic Analogy Using the Jet Engine Noise REduction (JENRE) Code. 55th AIAA Aerospace Sciences Meeting, American Institute of Aeronautics and Astronautics, Jan 05, 2017. https://doi.org/10.2514/6.2017-0459

[17] Markesteijn, A. P., and Karabasov, S. A. CABARET Solutions on Graphics Processing Units for NASA Jets: Grid Sensitivity and Unsteady Inflow Condition Effect. Comptes Rendus Mécanique, Elsevier BV, 346, 10, Oct, 2018, pp. 948–963. https://doi.org/10.1016/j.crme.2018.07.004

[18] Xia, H. Turbulent Jet Characteristics for Axisymmetric and Serrated Nozzles. Computers & Fluids, Elsevier BV, 110, Mar, 2015, pp. 189–197. https://doi.org/10.1016/j.compfluid.2014.09.035

[19] Housman, J. A., Stich, G.-D., and Kiris, C. C. Jet Noise Prediction Using Hybrid RANS/LES with Structured Overset Grids. 23rd AIAA/CEAS Aeroacoustics Conference, American Institute of Aeronautics and Astronautics, Jun 02, 2017. DOI: 10.2514/6.2017-3213

[20] Fuchs, M., Mockett, C., Shur, M., Strelets, M., and Kok, J. C. Single-Stream Round Jet at M = 0.9. Notes on Numerical Fluid Mechanics and Multidisciplinary Design, Springer International Publishing, Jul 27, 2017, pp. 125–137. DOI:10.1007/978-3-319-52995-0_6

[21] Wang, Z.-N., Tyacke, J., Tucker, P., and Boehning, P. Parallel Computation of Aeroacoustics of Industrially Relevant Complex-Geometry Aeroengine Jets. Computers & Fluids, Elsevier BV, 178, Jan, 2019, pp. 166–178. https://doi.org/10.1016/j.compfluid.2018.04.039

[22] van der Velden, W. C. P., Casalino, D., Gopalakrishnan, P., Jammalamadaka, A., Li, Y., Zhang, R., and Chen, H. Validation of Jet Noise Simulations and Resulting Insights of Acoustic Near Field. AIAA Journal, American Institute of Aeronautics and Astronautics (AIAA), 57, 12, Dec, 2019, pp. 5156–5167. https://doi.org/10.2514/1.j057970

[23] Rego, L., Avallone, F., Ragni, D., and Casalino, D. Jet-Installation Noise and near-Field Characteristics of Jet–Surface Interaction. Journal of Fluid Mechanics, Cambridge University Press (CUP), 895, May 12, 2020. https://doi.org/10.1017/jfm.2020.294

[24] Brès, G. A., Jordan, P., Jaunet, V., Le Rallic, M., Cavalieri, A. V. G., Towne, A., Lele, S. K., Colonius, T., and Schmidt, O. T. Importance of the Nozzle-Exit Boundary-Layer State in Subsonic Turbulent Jets. Journal of Fluid Mechanics, Cambridge University Press (CUP), 851, Jul 19, 2018, pp. 83–124. https://doi.org/10.1017/jfm.2018.476

[25] Lesshafft, L., Semeraro, O., Jaunet, V., Cavalieri, A. V. G., and Jordan, P. Resolvent-Based Modeling of Coherent Wave Packets in a Turbulent Jet. Physical Review Fluids, American Physical Society (APS), 4, 6, Jun 06, 2019. https://doi.org/10.1103/physrevfluids.4.063901

[26] Wang, Z.-N., Proenca, A., Lawrence, J., Tucker, P. G., and Self, R. Large-Eddy-Simulation Prediction of an Installed Jet Flow and Noise with Experimental Validation. AIAA Journal, American Institute of Aeronautics and Astronautics (AIAA), 58, 6, Jun, 2020, pp. 2494–2503. https://doi.org/10.2514/1.j058921

[27] Ffowcs Williams, J. E., Hawkings, D. L., Sound Generation by Turbulence and Surfaces in Arbitrary Motion. Philosophical Transactions of the Royal Society of London. Series A, Mathematical and Physical Sciences, The Royal Society, 264, 1151, May 08, 1969, pp. 321–342. https://doi.org/10.1098/rsta.1969.0031

[28] Goloviznin, V. M., Samarskii, A. A., Finite difference approximation of convective transport equation with space splitting time derivative, Jour Matem. Mod., 1998 , 10(1), 86–100.

[29] Karabasov, S. A., and Goloviznin, V. M. Compact Accurately Boundary-Adjusting High-REsolution Technique for Fluid Dynamics. Journal of Computational Physics, Elsevier BV, 228, 19, Oct, 2009, pp. 7426–7451. https://doi.org/10.1016/j.jcp.2009.06.037

[30] Chintagunta, A., Naghibi, S. E., and Karabasov, S. A. Flux-Corrected Dispersion-Improved CABARET Schemes for Linear and Nonlinear Wave Propagation Problems. Computers & Fluids, Elsevier BV, 169, Jun, 2018, pp. 111–128. https://doi.org/10.1016/j.compfluid.2017.08.018

[31] Semiletov, V. A., and Karabasov, S. A. CABARET Scheme with Conservation-Flux Asynchronous Time-Stepping for Nonlinear Aeroacoustics Problems. Journal of Computational Physics, Elsevier BV, 253, Nov, 2013, pp. 157–165. https://doi.org/10.1016/j.jcp.2013.07.008

[32] Markesteijn, A. P., and Karabasov, S. A. GPU CABARET Flow and Noise Solutions of an Installed Jet Configuration. AIAA AVIATION 2020 FORUM, American Institute of Aeronautics and Astronautics, Jun 08, 2020. 10.2514/6.2020-2563

[33] Markesteijn, A. P., and Karabasov, S. A. GPU CABARET Solutions for the NASA SHJAR Jet Noise Experiment: Flow and Noise Modeling. 23rd AIAA/CEAS Aeroacoustics Conference, American Institute of Aeronautics and Astronautics, Jun 02, 2017. https://doi.org/10.2514/6.2017-3852

[34] Markesteijn, A. P., Gryazev, V., Karabasov, S. A., Ayupov, R. Sh., Benderskiy, L. A., and Lyubimov, D. A. Flow and Noise Predictions of Coaxial Jets. AIAA Journal, American Institute of Aeronautics and Astronautics (AIAA), 58, 12, Dec, 2020, pp. 5280–5293. https://doi.org/10.2514/1.J058881

[35] Khavaran, A., and Bridges, J. Development of Jet Noise Power Spectral Laws Using SHJAR Data. 15th AIAA/CEAS Aeroacoustics Conference (30th AIAA Aeroacoustics Conference), American Institute of Aeronautics and Astronautics, May 11, 2009. https://doi.org/10.2514/6.2009-3378

[36] Gryazev, V., Markesteijn, A. P., and Karabasov, S. A. Generalized Acoustic Analogy Modeling of Hot Jet Noise. AIAA Journal, American Institute of Aeronautics and Astronautics (AIAA), 60, 4, Apr, 2022, pp. 2383–2396. https://doi.org/10.2514/1.J060896

[37] Gryazev, V., Markesteijn, A. P., and Karabasov, S. A. Robustness of Reduced-Order Jet Noise Models. AIAA Journal, American Institute of Aeronautics and Astronautics (AIAA), 61, 1, Jan, 2023, pp. 315–328. https://doi.org/10.2514/1.J061840

[38] Goldstein, M. E. A Unified Approach to Some Recent Developments in Jet Noise Theory. International Journal of Aeroacoustics, SAGE Publications, 1, 1, Jan, 2002, pp. 1–16. 10.1260/1475472021502640

[39] Goldstein, M. E. A Generalized Acoustic Analogy. Journal of Fluid Mechanics, Cambridge University Press (CUP), 488, Jul 10, 2003, pp. 315–333. https://doi.org/10.1017/S0022112003004890

[40] Goldstein, M.E., Leib, S. J., The Aero-acoustics of slowly diverging supersonic jets, Journal of Fluid Mechanics., Vol. 600, 2008. https://doi.org/10.1017/S0022112008000311

[41] Karabasov, S. A., Afsar, M. Z., Hynes, T. P., Dowling, A. P., McMullan, W. A., Pokora, C. D., Page, G. J., and McGuirk, J. J. Jet Noise: Acoustic Analogy Informed by Large Eddy Simulation. AIAA Journal, American Institute of Aeronautics and Astronautics (AIAA), 48, 7, Jul, 2010, pp. 1312–1325. 10.2514/1.44689

[42] Depuru Mohan, N. K., Dowling, A. P., Karabasov, S. A., Xia, H., Graham, O., Hynes, T. P., and Tucker, P. G. Acoustic Sources and Far-Field Noise of Chevron and Round Jets. AIAA Journal, American Institute of Aeronautics and Astronautics (AIAA), 53, 9, Sep, 2015, pp. 2421–2436. https://doi.org/10.2514/1.J052973

[43] Bridges, J. E. Simple Scaling Of Multi-Stream Jet Plumes For Aeroacoustic Modeling. 54th AIAA Aerospace Sciences Meeting, American Institute of Aeronautics and Astronautics, Jan 02, 2016. https://doi.org/10.2514/6.2016-1637

[44] Witze, P. O. Centerline Velocity Decay of Compressible Free Jets. AIAA Journal, American Institute of Aeronautics and Astronautics (AIAA), 12, 4, Apr, 1974, pp. 417–418. https://doi.org/10.2514/3.49262

[45] Towne, A., Cavalieri, A. V. G., Jordan, P., Colonius, T., Schmidt, O., Jaunet, V., and Brès, G. A. Acoustic Resonance in the Potential Core of Subsonic Jets. Journal of Fluid Mechanics, Cambridge University Press (CUP), 825, Jul 27, 2017, pp. 1113–1152. https://doi.org/10.1017/jfm.2017.346

[46] Park, G.I. 2015. “Wall-modeled large-eddy simulation of a separated flow over the NASA wall-mounted hump”, Center for Turbulence Research, Annual Research Briefs

[47] Saad, T., Cline, D., Stoll, R., and Sutherland, J. C. Scalable Tools for Generating Synthetic Isotropic Turbulence with Arbitrary Spectra. AIAA Journal, American Institute of Aeronautics and Astronautics (AIAA), 55, 1, Jan, 2017, pp. 327–331. https://doi.org/10.2514/1.J055230

[48] Richards, A., Saad, T., and Sutherland, J. C. A Fast Turbulence Generator Using Graphics Processing Units. 2018 Fluid Dynamics Conference, American Institute of Aeronautics and Astronautics, Jun 24, 2018. https://doi.org/10.2514/6.2018-3559

[49] Mukha, T., Rezaeiravesh, S., and Liefvendahl, M. A Library for Wall-Modelled Large-Eddy Simulation Based on OpenFOAM Technology. Computer Physics Communications, Elsevier BV, 239, Jun, 2019, pp. 204–224. https://doi.org/10.1016/j.cpc.2019.01.016

[50] Karabasov, S., Bogey, C., and Hynes, T. An Investigation of the Mechanisms of Sound Generation in Initially Laminar Subsonic Jets Using the Goldstein Acoustic Analogy. Journal of Fluid Mechanics, Cambridge University Press (CUP), 714, Jan 02, 2013, pp. 24–57. https://doi.org/10.1017/jfm.2012.448

[51] Tam, C.K.W., Auriault, L., "Mean flow refraction effects on sound from localized sources in a jet," Journal of Fluid Mechanics, Vol. 370, pp. 149-174, 1998. https://doi.org/10.1017/S0022112098001852

[52] Tam, C. K. W., and Auriault, L. Jet Mixing Noise from Fine-Scale Turbulence. AIAA Journal, American Institute of Aeronautics and Astronautics (AIAA), 37, 2, Feb, 1999, pp. 145–153. https://doi.org/10.2514/2.691

Jet flow and noise predictions for the Doak laboratory experiment

Gryazev, Vasily

2023-04-02

Gryazev V, Markesteijn AP, Karabasov SA, et al., (2023) Jet flow and noise predictions for the Doak laboratory experiment. AIAA Journal, Available online 2 April 2023
https://doi.org/10.2514/1.J062365 Sections Read Now